




Multi-Scale Modeling and Experimental Study of the Strength of Plain-Woven SiC/SiC Composites

Xiguang Gao^{1,2}  · Hongnian Dong^{1,2} · Sheng Zhang^{1,2} · Yingdong Song^{1,2,3}

Received: 23 March 2019 / Accepted: 12 August 2019 / Published online: 27 August 2019
© Springer Nature B.V. 2019

Abstract

The strength of plain-woven SiC/SiC composites was predicted with the multi-scale method. Firstly, a three-dimensional unit cell was used to characterize the geometric structure of plain-woven SiC/SiC composites. Secondly, the yarns were seen as minicomposites, whose axial mechanical properties were obtained by the shear-lag model, and the fiber defect model was adopted to simulate the failure process of minicomposites. The strength of plain-woven SiC/SiC composites predicted with the multi-scale method is in good agreement with the experimental result. Besides, the effects of heat treatment and load-carrying capacity of broken fiber on the strength of plain-woven SiC/SiC composites were evaluated, and the effect of woven geometry structure was also evaluated.

Keywords Ceramic matrix composites · Failure · Finite element analysis · Heat treatment · Strength · Multi-scale

1 Introduction

Fiber-reinforced ceramic matrix composites (CMCs) not only inherit ceramics' outstanding properties, such as high strength, high modulus, high hardness, chemically inert and high melting temperature but also overcome the brittleness and notch sensitivity of ceramics. Given

✉ Xiguang Gao
gaoxiguang@nuaa.edu.cn

✉ Yingdong Song
ydsong@nuaa.edu.cn

¹ Key Laboratory of Aero-engine Thermal Environment and Structure, Ministry of Industry and Information Technology, Nanjing 210016, People's Republic of China

² Jiangsu Province Key Laboratory of Aerospace Power System, College of Energy and Power Engineering, Nanjing University of Aeronautics and Astronautics, 29 Yudao St, Nanjing 210016, People's Republic of China

³ State Key Laboratory of Mechanics and Control Mechanical Structures, Nanjing University of Aeronautics and Astronautics, Nanjing 210016, People's Republic of China

the excellent properties, CMCs have been applied to aero-engine, automobile brake system, and other modern engineering structures [1–3]. According to the yarn structure, CMCs can be divided into unidirectional, cross-ply, and woven structures. Compared with unidirectional and cross-ply CMCs, woven CMCs possess better delamination resistance and impact tolerance, and have become the main form in engineering applications. Hence, the strength prediction of woven CMCs is an essential and critical task in the design of CMCs structures.

Curtin [4, 5] was the first to present a theory incorporating the statistical nature of the fiber strength and the presence of fiber/matrix sliding to predict the ultimate tensile strength of CMCs. Although the theory can only be applied to unidirectional CMCs, it also gives guidance for strength prediction of woven CMCs.

Although woven CMCs possess complex geometric structures, many significant signs of progress in modeling the mechanical behavior of woven CMCs have been made. The conventional methods include micromechanics-based approaches [6–9], continuum damage mechanics [10], and multi-scale methods [11, 12]. However, in the above studies, the strength of woven CMCs has not been predicted.

Jacobsen et al. [13] predicted stress-strain response and failure strength of plain-woven CMCs by using the theory of a cross-ply laminate. While the lamination theory did offer an efficient method to predict in-plane effective properties, the unit-cell micro-stress and micro-strain variations were shown to be more complicated than that assumed by the lamination theory. Limited in plane stress, the lamination theory cannot be applied to 3D woven CMCs. Yang et al. [14] formulated a new methodology for damage coupling analysis and characterized the damage coupling behavior and its effect on the failure strength of CMCs. However, the theory is a phenomenological analytical method based on experimental results. Hence, it cannot be used to analyze the failure process in micro-scale. Besides, some researchers have found that the strength of SiC fibers could be changed by the high-temperature process [15]. However, the in situ strength of SiC fibers has not been used to predict the strength of woven SiC/SiC composites.

By combining the minimum repeating unit of periodic structure with the micromechanical model, the multi-scale method can establish the relationship between the macroscopic mechanical behaviors of woven composites and the microscopic constituent properties and the microscopic geometry structures, and it has been the tendency of modeling the mechanical behavior of woven composites. The purpose of this paper is to predict the strength of plain-woven SiC/SiC composites with the multi-scale method. Firstly, a three-dimensional unit cell was used to characterize the geometric structure of plain-woven SiC/SiC composites. To avoid the adjacent warps being fastened together, a narrow gap was set between the adjacent warps. Secondly, the yarns were seen as minicomposites, whose axial mechanical properties were obtained by the shear-lag model. To simulate the failure process of minicomposites, the defect model proposed by Zhang et al. [16] was adopted, and it was assumed that global load redistribution occurred upon fiber fracturing [4]. The in situ strength distribution of SiC fibers was counted up to obtain the necessary experimental data for the fiber fracture model. The strength of plain-woven SiC/SiC composites predicted with the multi-scale method is in good agreement with the experimental result. Besides, the effects of heat treatment and load-carrying capacity of broken fiber on the strength of plain-woven SiC/SiC composites were evaluated, and the effect of woven geometry structure was also evaluated.

2 Material and Experimental Procedure

2.1 Tensile Tests of Plain-Woven SiC/SiC Composites

The manufacturing process of plain-woven SiC/SiC composites consisted of two steps. First, the preforms were manufactured with SiC fiber bundles (SLF-SiC-NF-10, Cerafil Ceramic Fiber Co., Ltd., Suzhou, China.), whose properties were similar to Nicalon™. Second, the SiC matrix was deposited through the CVI (Chemical Vapor Infiltration) technique at the temperature of 1100 °C for 500 h. Due to the low densification characteristic of CVI, there were lots of pores between the yarns, and the porosity was up to 34%.

Two plain-woven SiC/SiC specimens that were cut from the same plain-woven SiC/SiC plate were subjected to the uniaxial tensile tests. The specimens were cut into the shape of a dog bone (see Fig. 1) using high-pressure water jet cutting. Two aluminum stiffeners were glued to both ends of the specimens to prevent them from being crushed by the collet chucks of the testing machine.

The tensile tests of plain-woven SiC/SiC composites were performed on a hydraulic servo load-frame (Model 793, MTS Systems Corp., Eden Prairie, MN USA) at room temperature under a constant displacement rate of 0.05 mm/min. An extensometer with a gauge length of 25 mm was used to determine the gauge-section strains.

2.2 Tensile Tests of Monofilaments

The method used herein to measure the in situ strength distribution of SiC monofilaments was similar to that used by Zhang et al. [16, 17]. Tensile tests of SiC monofilaments were performed on a YG001B monofilament strength tester under a constant displacement rate of 10 mm/min. The gauge length of monofilament was 25 mm. At the preparation stage, the monofilaments were heat-treated in the tube furnace filled with Ar. The maximum heating temperature was 1100 °C, and the total heating time was 500 h. The heating process was the same as the fabrication process of plain-woven SiC/SiC composites so that the strength distribution of tested fibers could represent the in situ strength distribution of fibers in plain-woven SiC/SiC composites. Each monofilament was glued to a mounting tab that was made of cardboard for ease of holding. Before tension, the cardboard was burnt out at the middle to ensure the monofilament to bear the whole load.

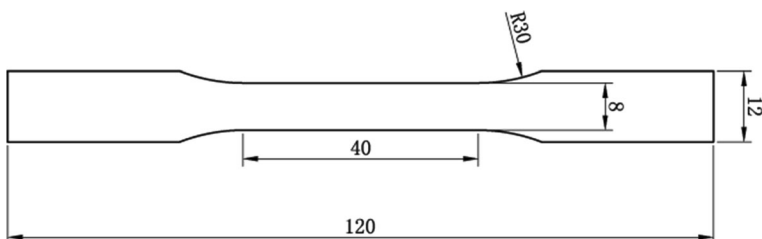


Fig. 1 Specimen dimension of plain-woven SiC/SiC composites

3 Modeling of Mechanical Behavior of Minicomposites

The primary damage and failure modes that dominate the mechanical behavior of minicomposites include matrix cracking, interfacial debonding, and fiber failure.

(a) Matrix cracking

The matrix crack spacing L can be determined by [18].

$$\frac{1}{L} = \frac{1}{L_{\text{sat}}} \left\{ 1 - \exp \left[- \left(\frac{\sigma}{\sigma_0} \right)^m \right] \right\} \tag{1}$$

where L is the matrix crack spacing, L_{sat} is the saturated matrix crack spacing, σ_0 and m are the statistical parameters.

(b) Interfacial debonding

Based on the shear-lag model [3], the fiber stress distribution can be described by

$$\sigma_f(x) = \begin{cases} \frac{\sigma}{v_f} - \frac{2\tau}{r_f} \left(\frac{L}{2} - x \right), & \frac{L}{2} - d \leq x \leq \frac{L}{2} \\ \sigma_{f0}, & 0 \leq x \leq \frac{L}{2} - d \end{cases} \tag{2}$$

where σ is the minicomposite stress; v_f is the fiber volume fraction; τ is the interfacial shear stress; r_f is the diameter of the fiber.

The length of the debonding region d can be described by

$$d = \left(\frac{\sigma}{v_f} - \sigma_{f0} \right) \frac{r_f}{2\tau} \tag{3}$$

The stress of fiber at the bonding region can be described by

$$\sigma_{f0} = \frac{E_f}{E_f v_f + E_m v_m} \sigma + E_f \left(\frac{\alpha_f v_f E_f + \alpha_m v_m E_m}{E_f v_f + E_m v_m} - \alpha_f \right) \Delta T \tag{4}$$

where E_f and E_m are the elastic modulus of fiber and matrix, respectively; v_m is the matrix volume fraction, α_f and α_m are the coefficient of thermal expansion of fiber and matrix, respectively; ΔT is the variation between the room temperature and the manufacturing temperature.

The composite’s average strain $\bar{\varepsilon}_c$ can be determined by

$$\begin{aligned} \bar{\varepsilon}_c &= \bar{\varepsilon}_f = \frac{2}{E_f L} \int_0^{L/2} \sigma_f(x) dx - \left(\frac{\alpha_f v_f E_f + \alpha_m v_m E_m}{E_c} - \alpha_f \right) \Delta T \\ &= \frac{2}{E_f L} \left[\frac{\sigma}{v_f} d - \frac{\tau}{r_f} d^2 + \sigma_{f0} \left(\frac{L}{2} - d \right) \right] - \left(\frac{\alpha_f v_f E_f + \alpha_m v_m E_m}{E_c} - \alpha_f \right) \Delta T \end{aligned} \tag{5}$$

(c) Fiber failure

To simulate fiber failure, the defect model proposed by Zhang et al. [16] was adopted. The defects of fibers were divided into n kinds, and the actual fracture strength of fibers caused by the j^{th} kind of defect was named as σ_j ($\sigma_1 < \dots < \sigma_j < \dots < \sigma_n$).

It was assumed that the j^{th} ($j = 1 \dots n$) kind of defect was randomly distributed, and the probability of appearing at the arbitrary place was the same. Each fiber was uniformly divided into $N_{\Delta l}$ segment, and the length of each segment was Δl . The incident that the i^{th} segment had the j^{th} kind of defect was named as A_j^i . If each defect was independent, P_j could be used to represent for $P(A_j^i)$ which was the probability that the incident A_j^i may happen.

If A_j was used to represent for the incident that the fiber with length of L had the j^{th} kind of defect, the probability that A_j may happen would be

$$P(A_j) = P\left(\cup_i A_j^i\right) = 1 - P\left(\cap_i \bar{A}_j^i\right) = 1 - \prod_i [1 - P(A_j^i)] = 1 - (1 - P_j)^{N_{\Delta l}} \tag{6}$$

Herein, set theory was adopted. \cup is the union operation. \cap is the intersection operation. \bar{A}_j^i represents the incident that the i^{th} segment did not have the j^{th} kind of defect.

If B_j was used to represent for the incident that the strength of the fiber with a length of L was σ_j , the probability that B_j may happen would be

$$P(B_j) = P\left(A_j \cap_{k=0}^{j-1} \bar{A}_k\right) = P(A_j) \cdot \prod_{k=0}^{j-1} [1 - P(A_k)] \tag{7}$$

Tensile tests were conducted on N_L fibers with a length of L , and the strength of each specimen was recorded as σ_i^* ($i = 1 \dots N_L$). Then, find out the minimum strength σ_{\min}^* and the maximum strength σ_{\max}^* . Divide the region between σ_{\min}^* and σ_{\max}^* into n equal sections. The average strength of each section was σ_j . After that, count up the sample size c_j of each section. Then

$$P(B_j) = c_j / N_L \quad j = 1, \dots, n \tag{8}$$

Based on Eq. (7), the formula of $P(A_j)$ could be derived.

$$P(A_j) = P(B_j) / \prod_{k=0}^{j-1} [1 - P(A_k)] \tag{9}$$

Base on Eq. (6), the probability that the fiber with a length of Δl had the j^{th} kind of defect could be calculated.

$$P_j = 1 - [1 - P(A_j)]^{1/N_{\Delta l}} \tag{10}$$

Herein, the Monte Carlo method was used to generate random numbers obeying uniform distribution for each segment. If the random number were smaller than the probability of the j^{th} kind of defect happening, this segment would be seen to have the j^{th} kind of defect. If this segment had the j^{th} kind of defect and did not have a more severe defect, the strength of this segment would be equal to σ_j (see Fig. 2). Compare the strength with its stress distribution for each segment, and the fiber failure process could be simulated.

It was assumed that global load redistribution occurs upon fiber failure [4]. Once the fiber broke at some point, the fiber stress at this point would rapidly drop to zero. However, to

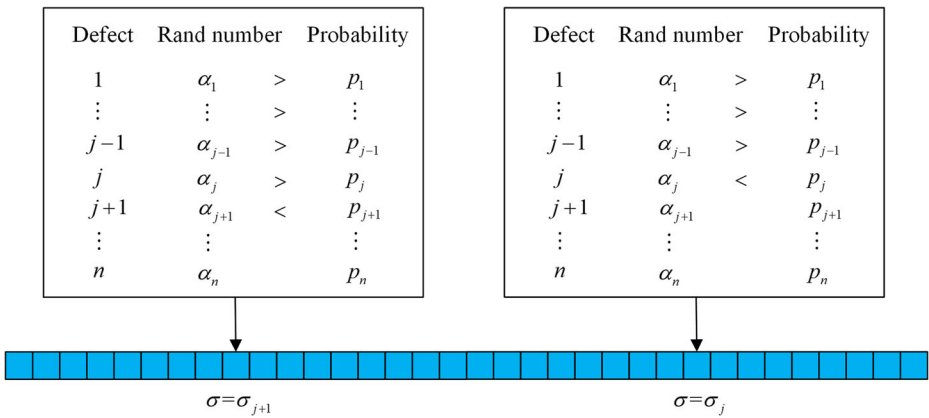


Fig. 2 Schematic diagram of determining fiber segment strength

understand the failure process better, a slow-motion was given to the failure process, then the fiber stress at the breakpoint could be seen to decrease step by step. At first, the fiber stress at the breakpoint only decreased by a very small value, and the fiber stress nearby would show an upward tendency through the interface shear stress transfer (see Fig. 3). The sliding region would increase step by step until the fiber stress dropped to zero at the breakpoint.

4 Modeling of Mechanical Behavior of Plain-Woven SiC/SiC Composites

4.1 Unit Cell Model

To obtain the mechanical behavior of plain-woven SiC/SiC composites, the multi-scale method was used by combining the unit cell model with the micromechanical model together. The minimum repeating unit of the periodic structure was chosen as the representative volume element, and its average mechanical behavior was seen as mechanical behavior of composites.

Based on the features of composite microstructure, some assumptions were made:

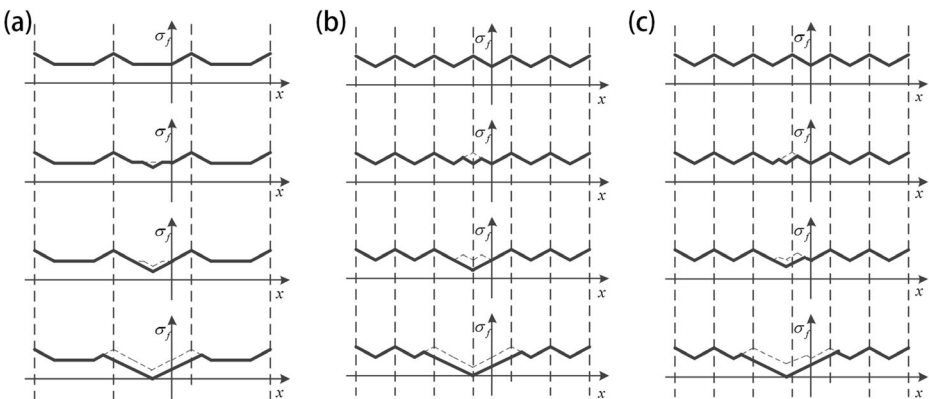


Fig. 3 Schematic diagram of fiber stress distribution during fiber failure process: (a) fiber broke at bonding region, (b) fiber broke at matrix cracking region, and (c) fiber broke at debonding region

- (a) The plain-woven SiC/SiC composites were composed of warps and wefts, and what between yarns was all pores;
- (b) The curve of warp in the axial direction was a trigonometric function;
- (c) The weft in the axial direction was straight;
- (d) The cross-section of yarns was a rectangle.

Based on the above assumptions, microscopic geometric parameters, including wavelength and amplitude of warp, the width of yarn's cross-section and height of warp's cross-section were obtained by measuring its three views (see Table 1).

Figure 4 shows the unit cell model of plain-woven SiC/SiC composites. Because the adjacent warps are actually not fastened together, during the modeling process, a narrow gap was set between the adjacent warps. The wefts and warps were assumed to be perfectly bonded. Research on frictional sliding between weft yarns and warp yarns is in progress.

Figure 5 shows the finite element model that included 24,935 tetrahedron elements and 7759 nodes. Both the unit cell model and finite element model were established in the commercial finite element software. The finite element grid information was exported to an ASCII file in a particular format. In the calculation process, this information would be imported into a self-compiled program with C language. The algorithm is described in the following sections.

4.2 Periodic Boundary Conditions

The load was applied to the unit cell in terms of periodic displacement boundary conditions [19].

$$u_{i+} - u_{i-} = \bar{\varepsilon}_{ij} \Delta x_j \quad (11)$$

where u_{i+} and u_{i-} are the displacements of a couple of boundary surfaces of the unit cell in the direction of i ; $\bar{\varepsilon}_{ij}$ is the average strain of the unit cell; Δx_j is the coordinate difference of the couple of boundary surfaces in the direction of j .

4.3 Element Stress

The yarn elements were seen as transverse isotropy material. The modulus along the yarn direction was modeled by the micromechanical model described in Section 3, and the concrete expression could be described by

$$E_1 = \frac{\sigma}{\bar{\varepsilon}_c} \quad (12)$$

Table 1 Microscopic geometric parameters of the unit cell of plain-woven SiC/SiC composites

Item	Value (mm)
Wave length of warp	9.72
Amplitude of warp	0.21
Width of yarn's cross-section	1.28
Height of warp's cross-section	0.24

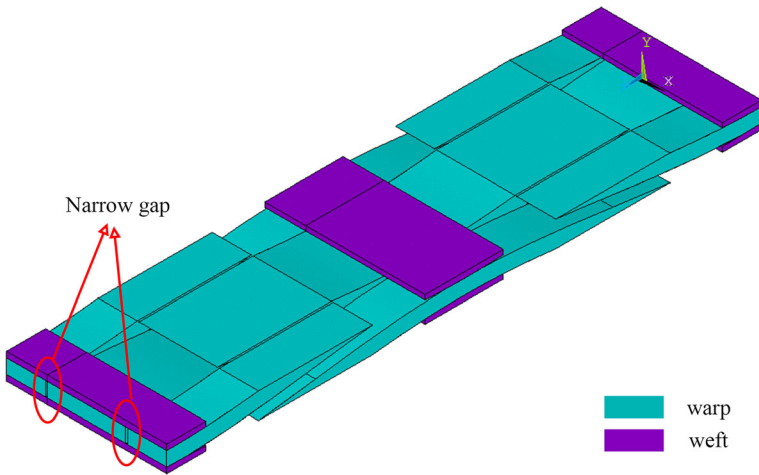


Fig. 4 Unit cell model of plain-woven SiC/SiC composites

where σ is the nominal stress of yarns; $\bar{\epsilon}_c$ is the average strain of yarns. $\bar{\epsilon}_c$ can be calculated by Eq. (5). The modulus perpendicular to the yarn direction is a constant. Based on the above analysis, the yarn element stiffness matrix could be easily obtained.

However, there was a certain angle between the principal directions of yarns and the principal axis of the unit cell, and the strain transformation matrix was used to transform the element stiffness matrix of warps.

$$\mathbf{D}_T = \mathbf{T}^T \mathbf{D} \mathbf{T} \tag{13}$$

Herein, \mathbf{T} is the strain transformation matrix; \mathbf{T}^T is the transposed vector of strain transformation matrix; \mathbf{D} is the original element stiffness matrix; \mathbf{D}_T is the transformed one.

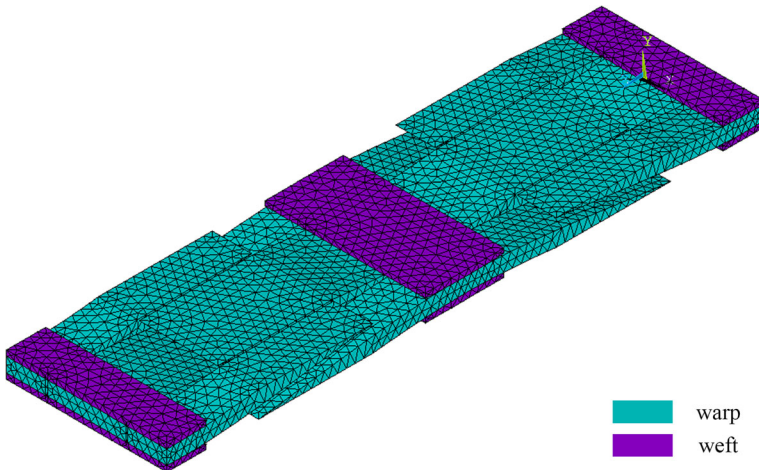


Fig. 5 Finite element model of plain-woven SiC/SiC composites

$$\mathbf{T} = \begin{bmatrix} l_1^2 & m_1^2 & n_1^2 & m_1 n_1 & n_1 l_1 & l_1 m_1 \\ l_2^2 & m_2^2 & n_2^2 & m_2 n_2 & n_2 l_2 & l_2 m_2 \\ l_3^2 & m_3^2 & n_3^2 & m_3 n_3 & n_3 l_3 & l_3 m_3 \\ 2l_2 l_3 & 2m_2 m_3 & 2n_2 n_3 & (m_2 n_3 + m_3 n_2) & (n_2 l_3 + n_3 l_2) & (l_2 m_3 + l_3 m_2) \\ 2l_3 l_1 & 2m_3 m_1 & 2n_3 n_1 & (m_3 n_1 + m_1 n_3) & (n_3 l_1 + n_1 l_3) & (l_3 m_1 + l_1 m_3) \\ 2l_1 l_2 & 2m_1 m_2 & 2n_1 n_2 & (m_1 n_2 + m_2 n_1) & (n_1 l_2 + n_2 l_1) & (l_1 m_2 + l_2 m_1) \end{bmatrix}. \text{ Here-}$$

in, l_i , m_i and n_i are the direction cosines between the principal directions of yarns and the principal axis of the unit cell (see Fig. 6), respectively.

The element stress can be calculated by

$$\sigma_e = \mathbf{D}_T \varepsilon_e \tag{14}$$

4.4 Average Stress

Now that each element stress had been calculated, the average stress of the unit cell could be calculated using the volume average method.

$$\bar{\sigma} = \frac{1}{V} \int_V \sigma_e^i dV \tag{15}$$

Herein, V is the volume of the unit cell, and σ_e^i is the stress of the i^{th} element.

4.5 Multi-Scale Modeling Process

For convenience, neither the friction between adjacent warps nor the friction between warps and wefts was considered. The relevant study about this aspect will be the focus in the future.

Herein, the mechanical behavior of warps and wefts was the critical point. In terms of wefts, along the warp direction, fiber and matrix connected in series to bear the load, and the bearing capacity was feeble. It was assumed that once the wefts bore the load along the warp direction, their transverse stiffness would reduce to a small value. Hence, the failure process of warp elements was the focus of the whole multi-scale modeling process.

Because the strength of each warp element was very close, single warp element failure would lead to a large number of elements to fail like the domino. Hence, once a single warp element failed, the plain-woven SiC/SiC composites were considered to fail. The strength of warp elements is much higher than the nonlinear critical stress. Hence, the domino failure of

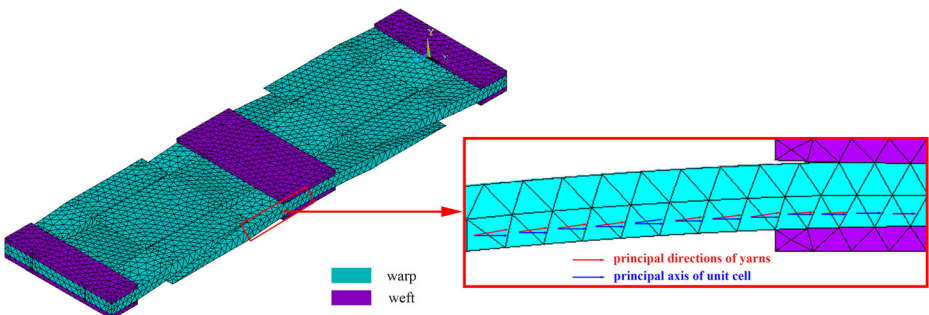


Fig. 6 Schematic diagram of the principal directions of yarns and the principal axis of unit cell

single warp element would not affect the largely nonlinear stress-strain curves of plain-woven SiC/SiC composites. The flow chart of the multi-scale modeling process is provided in Fig. 7.

5 Results and Discussion

5.1 Evaluation of the Strength of Plain-Woven SiC/SiC Composites

The microscopic material properties of yarns are provided in Table 2. The definition of these material parameters can refer to Eq. 1–5 in Section 3. The macroscopic material properties of yarns perpendicular to the yarn direction are provided in Table 3.

As mentioned above, the strength of SiC fibers could be changed by the high-temperature process [15]. Damage could be inevitably incorporated into SiC fibers during the fabrication process. Hence, the statistical strength of SiC monofilaments after heat treatment (see Fig. 8) was adopted to obtain accurate analysis results, and the theoretical model can refer to Eq. 6–10 in Section 3.

The stress-strain response and strength of plain-woven SiC/SiC composites are presented in Fig. 9. It can be seen that the dispersion of the experimental results is very small, and the present analysis and the experimental results are in good agreement. Note that the average

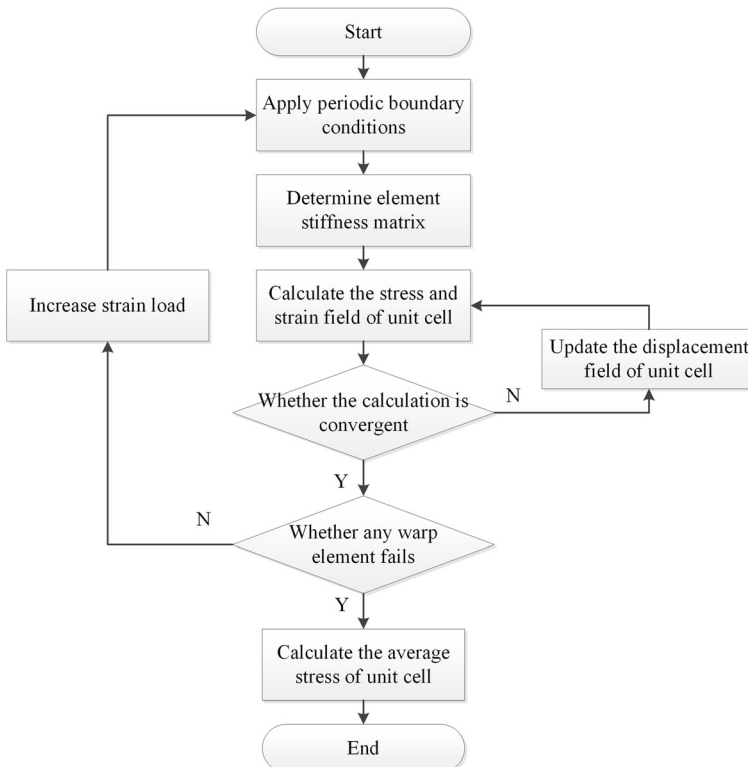


Fig. 7 Flow chart of multi-scale modeling process of the strength of plain-woven SiC/SiC composites

Table 2 Microscopic material properties of yarns

Item	Value	Item	Value
E_f (GPa)	146	E_m (GPa)	312
ν_f	0.425	ν_m	0.575
r_f (μm)	6.5	τ (MPa)	17
L_{sat} (mm)	0.25	σ_0 (MPa)	375
m	4	ΔT ($^{\circ}\text{C}$)	-1000
α_f ($\times 10^{-6}/^{\circ}\text{C}$)	3.1	α_m ($\times 10^{-6}/^{\circ}\text{C}$)	4.6

strength of experimental results 1 and experimental results 2 is 318.8 MPa, and the strength from present analysis is 300.3 MPa. The relative error is about 5.8%.

5.2 Effect of Heat Treatment

To evaluate the effect of heat treatment on the mechanical behavior of plain-woven SiC/SiC composites, the statistical strength of SiC monofilament before heat treatment (see Fig. 10) was also adopted in this Section. All the parameter values except SiC statistical strength were the same as that in section 5.1.

The stress-strain response and strength of plain-woven SiC/SiC composites predicted with the statistical strength of SiC monofilaments before and after heat treatment are presented in Fig. 11. The strength predicted with the statistical strength of SiC monofilaments after heat treatment is 300.3 MPa, and the strength predicted with the statistical strength of SiC monofilaments before heat treatment is 520.3 MPa. The latter is much higher than the former, and the latter is in good agreement with the experimental results. The reason may be that the SiC monofilaments after heat treatment have much lower strength than the ones before heat treatment, and the strength of SiC monofilaments after heat treatment is approximately equal to the in situ strength.

5.3 Effect of Load-Carrying Capacity of Broken Fiber

In this section, the effect of the load-carrying capacity of broken fiber was evaluated. All the parameter values were the same as that in section 5.1.

The stress-strain response and strength of plain-woven SiC/SiC composites predicted with and without the load-carrying capacity of the broken fiber are presented in Fig. 12. The strength predicted without the load-carrying capacity of the broken fiber is 136.6 MPa, and the strength predicted with the load-carrying capacity of the broken fiber is 300.3 MPa. The former is much lower than the latter, and the latter is in good agreement with the experimental results. The reason may be that the latter was based on the assumption that the broken fiber could still carry load where away from the breakpoint, and this assumption was consistent with reality.

Table 3 Macroscopic material properties of yarns [20] perpendicular to the yarn direction

E_2 (GPa)	E_3 (GPa)	G_{12} (Gpa)	G_{13} (Gpa)	ν_{12}	ν_{13}
130.18	130.18	60.5	60.5	0.178	0.178

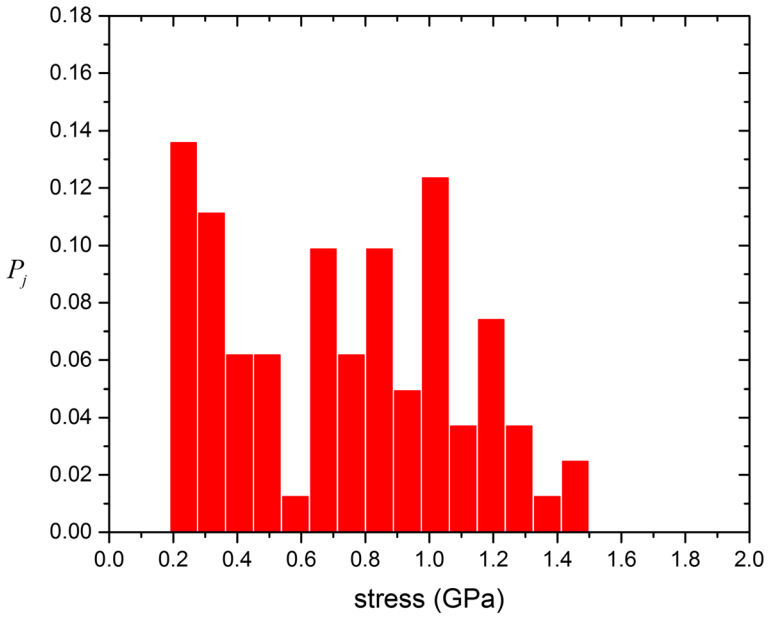


Fig. 8 Statistical strength of SiC monofilament after heat treatment

5.4 Effect of Woven Geometry Structure

The stress-strain response and strength of plain-woven composites with different wavelength of warp were analyzed to evaluate the effect of woven geometry structure.

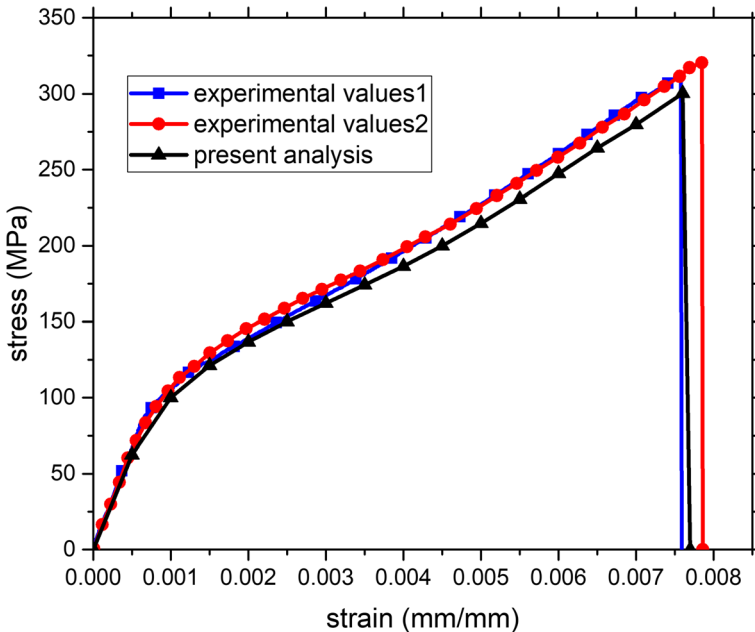


Fig. 9 Stress-strain response and strength of plain-woven SiC/SiC composites

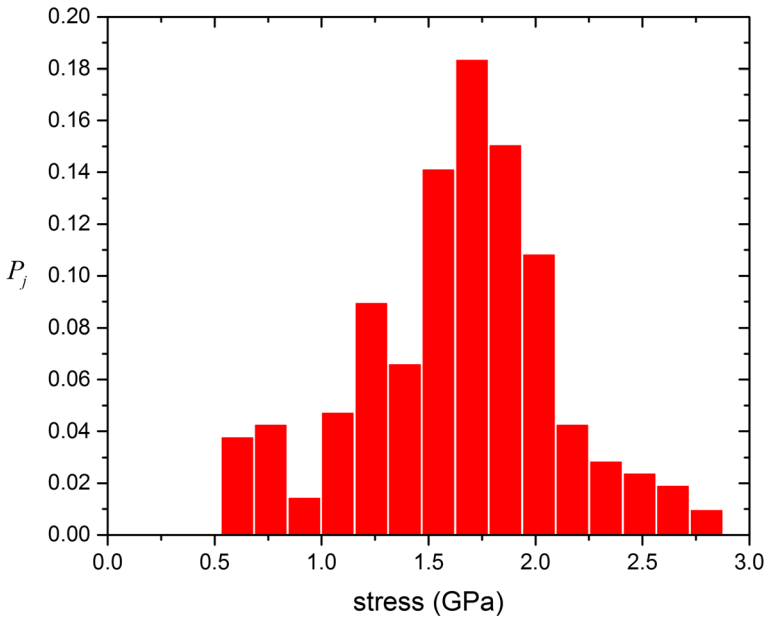


Fig. 10 Statistical strength of SiC monofilament before heat treatment

Here, all the parameter values except the wavelength of the warp were the same as that in section 5.1, and the wavelength of the warp was 7.776, 9.720, and 11.664, respectively.

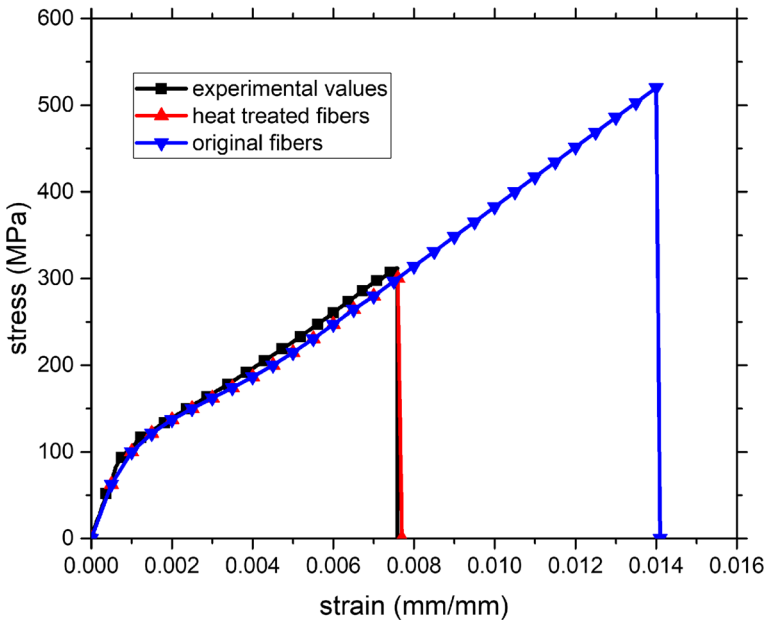


Fig. 11 Stress-strain response and strength of plain-woven SiC/SiC composites predicted with the statistical strength of SiC monofilament before and after heat treatment

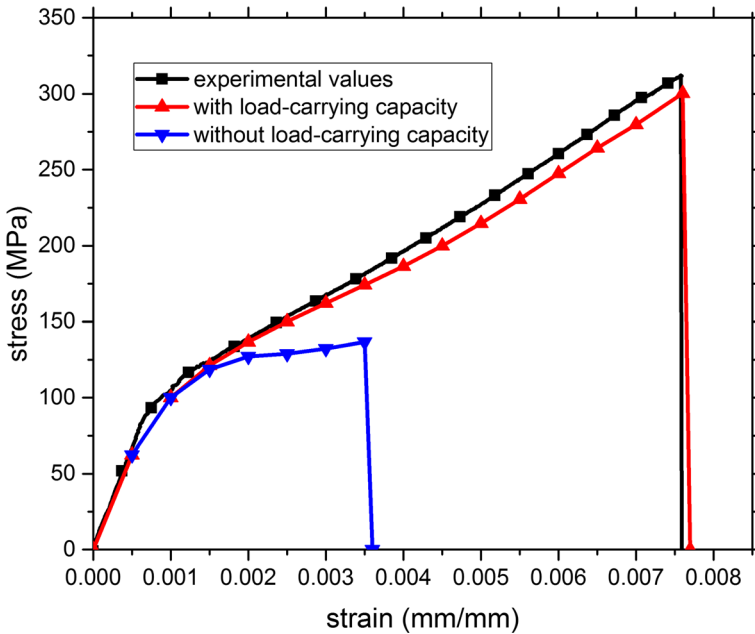


Fig. 12 Stress-strain response and strength of plain-woven SiC/SiC composites predicted with and without load-carrying capacity of broken fiber

The stress-strain response and strength of plain-woven composites with the different wavelength of warp are presented in Fig. 13. With the decrease in wavelength of warps, the stress of composites also decreased. However, when the wavelength of warps decreased, the strength of composites increased. The reason may be as follow. The decrease in wavelength leads the warp to bend more severely. The stiffness of warp in the direction parallel with fibers is higher than the stiffness in the direction vertical with fibers, so the stiffness of warp is equivalently weakened. However, when the wavelength decreased, the failure strain of composites increased, which, as a whole lead to the increase of strength.

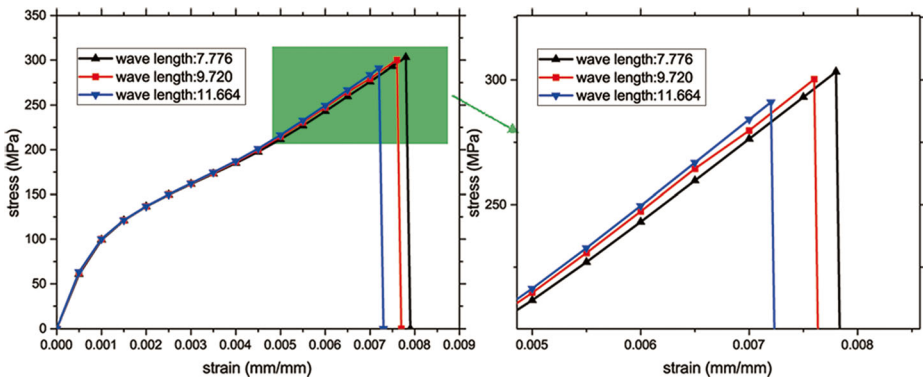


Fig. 13 Stress-strain response and strength of plain-woven composites with difference wave length of warp

6 Conclusions

In this paper, the strength of plain-woven SiC/SiC composites was predicted with the multi-scale method. Firstly, a three-dimensional unit cell was used to characterize the geometric structure of plain-woven SiC/SiC composites. Secondly, the yarns were seen as minicomposites, whose axial mechanical properties were obtained by the shear-lag model, and the fiber defect model was adopted to simulate the failure process of minicomposites. The strength of plain-woven SiC/SiC composites predicted with the multi-scale method is in good agreement with the experimental result. Some conclusions can be obtained as follows:

- (1) The strength predicted with the statistical strength of SiC monofilament before heat treatment is much higher than the strength predicted with the statistical strength of SiC monofilament after heat treatment, and the latter is in good agreement with the experimental results. The reason may be that the SiC monofilaments after heat treatment have much lower strength than the ones before heat treatment, and the strength of SiC monofilaments after heat treatment is approximately equal to the in situ strength.
- (2) The strength predicted without the load-carrying capacity of the broken fiber is much lower than the strength predicted with the load-carrying capacity of the broken fiber, and the latter is in good agreement with the experimental results. The reason may be that the latter was based on the assumption that the broken fiber could still carry load where away from the breakpoint, and this assumption was consistent with reality.
- (3) With the decrease in the wavelength of warps, the stress of composites also decreased. However, when the wavelength of warps decreased, the strength of composites increased. The reason may be as follow. The decrease in wavelength leads the warp to bend more severely. The stiffness of warp in the direction parallel with fibers is higher than the stiffness in the direction vertical with fibers, so the stiffness of warp is equivalently weakened. However, when the wavelength decreased, the failure strain of composites increased, which, as a whole lead to the increase of strength.

Acknowledgements This work was supported by the National Key Research and Development Program of China [grant number 2017YFB0703200], the National Natural Science Foundation of China [grant numbers 51575261, 51675266], the Fundamental Research Funds for the Central universities [NF2018002], and the Priority Academic Program Development of Jiangsu Higher Education Institutions.

References

1. Yin, X.W., Cheng, L.F., Zhang, L.T., Travitzky, N., Greil, P.: Fibre-reinforced multifunctional SiC matrix composite materials. *Int. Mater. Rev.* **62**(3), 117–172 (2017). <https://doi.org/10.1080/09506608.2016.1213939>
2. Meyer, P., Waas, A.M.: FEM predictions of damage in continous fiber ceramic matrix composites under transverse tension using the crack band method. *Acta Mater.* **102**, 292–303 (2016). <https://doi.org/10.1016/j.actamat.2015.09.002>
3. Gao, X.G., Zhang, S., Fang, G.W., Song, Y.D.: Distribution of slip regions on the fiber-matrix interface of ceramic matrix composites under arbitrary loading. *J. Reinf. Plast. Compos.* **34**(20), 1713–1723 (2015). <https://doi.org/10.1177/0731684415596596>
4. Curtin, W.A.: Theory of mechanical properties of ceramic-matrix composites. *J. Am. Ceram. Soc.* **74**(11), 2837–2845 (1991). <https://doi.org/10.1111/j.1151-2916.1991.tb06852.x>

5. Curtin, W.A.: Ultimate strengths of fibre-reinforced ceramics and metals. *Composites*. **24**(2), 98–102 (1993). [https://doi.org/10.1016/0010-4361\(93\)90005-s](https://doi.org/10.1016/0010-4361(93)90005-s)
6. Keith, W.P., Kedward, K.T.: The stress-strain behaviour of a porous unidirectional ceramic matrix composite. *Composites*. **26**(3), 163–174 (1995). [https://doi.org/10.1016/0010-4361\(95\)91379-j](https://doi.org/10.1016/0010-4361(95)91379-j)
7. Pryce, A.W., Smith, P.A.: Matrix cracking in unidirectional ceramic matrix composites under quasi-static and cycle loading. *Acta Metall. Mater.* **41**(4), 1269–1281 (1993). [https://doi.org/10.1016/0956-7151\(93\)90178-u](https://doi.org/10.1016/0956-7151(93)90178-u)
8. Curtin, W.A., Ahn, B.K., Takeda, N.: Modeling brittle and tough stress-strain behavior in unidirectional ceramic matrix composites. *Acta Mater.* **46**(10), 3409–3420 (1998). [https://doi.org/10.1016/s1359-6454\(98\)00041-x](https://doi.org/10.1016/s1359-6454(98)00041-x)
9. Yang, C.P., Jia, F., Wang, B., Huang, T., Jiao, G.Q.: Unified tensile model for unidirectional ceramic matrix composites with degraded fibers and interface. *J. Eur. Ceram. Soc.* **39**(2–3), 222–228 (2019). <https://doi.org/10.1016/j.jeurceramsoc.2018.09.006>
10. Aubard, X., Lamon, J., Allix, O.: Model of the nonlinear mechanical behavior of 2D SiC-SiC chemical vapor infiltration composites. *J. Am. Ceram. Soc.* **77**(8), 2118–2126 (1994). <https://doi.org/10.1111/j.1151-2916.1994.tb07106.x>
11. Fagianò, C., Genet, M., Baranger, E., Ladeveze, P.: Computational geometrical and mechanical modeling of woven ceramic composites at the mesoscale. *Compos. Struct.* **112**, 146–156 (2014). <https://doi.org/10.1016/j.compstruct.2014.01.045>
12. Ismar, H., Schroter, F., Streicher, F.: Modeling and numerical simulation of the mechanical behavior of woven SiC/SiC regarding a three-dimensional unit cell. *Comput. Mater. Sci.* **19**(1–4), 320–328 (2000). [https://doi.org/10.1016/s0927-0256\(00\)00170-1](https://doi.org/10.1016/s0927-0256(00)00170-1)
13. Jacobsen, T.K., Brondsted, P.: Mechanical properties of two plain-woven chemical vapor infiltrated silicon carbide-matrix composites. *J. Am. Ceram. Soc.* **84**(5), 1043–1051 (2001). <https://doi.org/10.1111/j.1151-2916.2001.tb00788.x>
14. Yang, C.P., Jiao, G.Q., Wang, B., Huang, T., Guo, H.B.: Damage-based failure theory and its application to 2D-C/SiC composites. *Compos. Pt. A-Appl. Sci. Manuf.* **77**, 181–187 (2015). <https://doi.org/10.1016/j.compositesa.2015.07.003>
15. Araki, H., Suzuki, H., Yang, W., Sato, S., Noda, T.: Effect of high temperature heat treatment in vacuum on microstructure and bending properties of SiCf/SiC composites prepared by CVI. *J. Nucl. Mater.* **258**, 1540–1545 (1998). [https://doi.org/10.1016/s0022-3115\(98\)00293-1](https://doi.org/10.1016/s0022-3115(98)00293-1)
16. Zhang, S., Gao, X.G., Song, Y.D.: In situ strength model for continuous fibers and multi-scale modeling the fracture of C/SiC composites. *Appl. Compos. Mater.* **26**(1), 357–370 (2019). <https://doi.org/10.1007/s10443-018-9696-y>
17. Zhang, S., Gao, X.G., Dong, H.N., Ju, X.R., Song, Y.D.: In situ modulus and strength of carbon fibers in C/SiC composites. *Ceram. Int.* **43**(9), 6885–6890 (2017). <https://doi.org/10.1016/j.ceramint.2017.02.109>
18. Zhang, S., Gao, X., Chen, J., Dong, H., Song, Y., Zhang, H.: Effects of micro-damage on the nonlinear constitutive behavior of SiC/SiC Minicomposites. *J. Ceram. Sci. Technol.* **7**(4), 341–347 (2016). <https://doi.org/10.4416/jcst2016-00040>
19. Xia, Z.H., Zhou, C.W., Yong, Q.L., Wang, X.W.: On selection of repeated unit cell model and application of unified periodic boundary conditions in micro-mechanical analysis of composites. *Int. J. Solids Struct.* **43**(2), 266–278 (2006). <https://doi.org/10.1016/j.ijsolstr.2005.03.055>
20. Gowayed, Y., Ojard, G., Santhosh, U., Jefferson, G.: Modeling of crack density in ceramic matrix composites. *J. Compos. Mater.* **49**(18), 2285–2294 (2015). <https://doi.org/10.1177/0021998314545188>

Publisher's Note Springer Nature remains neutral with regard to jurisdictional claims in published maps and institutional affiliations.